This article was downloaded by:
On: *25 January 2011*
Access details: *Access Details: Free Access*
Publisher *Taylor & Francis*
Informa Ltd Registered in England and Wales Registered Number: 1072954 Registered office: Mortimer House, 37-41 Mortimer Street, London W1T 3JH, UK

Separation Science and Technology
Publication details, including instructions for authors and subscription information:
http://www.informaworld.com/smpp/title~content=t713708471

Frequency Response of the Back-flow Cell Model of Mass-Transfer Processes: Packed-Column Characteristics for Tracer-Gas Absorption

C. V. McSwain[ab]; L. D. Durbin[a]
[a] Department of Chemical, Engineering Texas A&M University, College Station, Texas [b] Humble Oil and Refining Co., Baytown, Texas

To cite this Article McSwain, C. V. and Durbin, L. D.(1969) 'Frequency Response of the Back-flow Cell Model of Mass-Transfer Processes: Packed-Column Characteristics for Tracer-Gas Absorption', Separation Science and Technology, 4: 1, 25 — 50
To link to this Article: DOI: 10.1080/01496396908052235
URL: http://dx.doi.org/10.1080/01496396908052235

PLEASE SCROLL DOWN FOR ARTICLE

Full terms and conditions of use: http://www.informaworld.com/terms-and-conditions-of-access.pdf

This article may be used for research, teaching and private study purposes. Any substantial or systematic reproduction, re-distribution, re-selling, loan or sub-licensing, systematic supply or distribution in any form to anyone is expressly forbidden.

The publisher does not give any warranty express or implied or make any representation that the contents will be complete or accurate or up to date. The accuracy of any instructions, formulae and drug doses should be independently verified with primary sources. The publisher shall not be liable for any loss, actions, claims, proceedings, demand or costs or damages whatsoever or howsoever caused arising directly or indirectly in connection with or arising out of the use of this material.

SEPARATION SCIENCE, 4(1), pp. 25–50, February, 1969

Frequency Response of the Back-flow Cell Model of Mass-Transfer Processes: Packed-Column Characteristics for Tracer-Gas Absorption

C. V. McSWAIN* and L. D. DURBIN

DEPARTMENT OF CHEMICAL ENGINEERING
TEXAS A&M UNIVERSITY
COLLEGE STATION, TEXAS

Downloaded At: 14:42 25 January 2011

Summary

Frequency-response techniques are developed for the backflow cell model as applied to countercurrent two-phase flow processes with exchange of a single solute. Experimental outlet-gas response curves have been obtained for step injection of tracer gas into the air inlet of a six-inch packed bubble column with different countercurrent flow rates of water. Numerical Fourier transformation of these curves yields frequency-response characteristics that are compared with those of the backflow cell model. On this basis, the backflow cell model adequately simulates the dynamics of the system.

In a previous article (*1*), the backflow cell model was introduced to describe continuous two-phase flow processes with imperfect axial mixing. Efficient computational methods of determining the solute-concentration profile in each phase and the efficiency of these processes at steady state were developed and discussed.

The schematic diagram of the backflow cell model is repeated here as Fig. 1 for a convenient reference. Each phase is considered to flow through a train of N perfectly mixed cells or stages with backflow, f_x or f_y, from each downstream cell to its neighbor upstream. Between adjacent cells of the different phases, the mass-transfer operation is

* Present address: Humble Oil and Refining Co., Baytown, Texas.

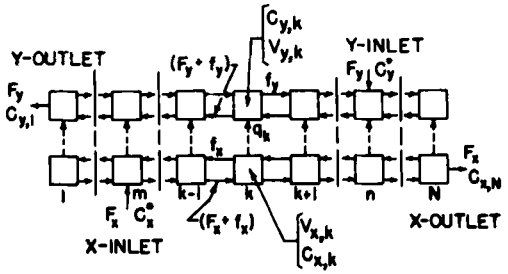

FIG. 1. Backflow cell model of two-phase countercurrent transfer operation.

that of a single solute between the rate-controlling or X phase and the Y phase. The rate of transfer is taken to be dependent upon the deviation from equilibrium in the X phase due to the concentration of solute in the Y phase. With respect to the kth cell, this rate is given by

$$q_k = k_{ox} a_k V_k (c_{x,k} - c^*_{x,k}) \tag{1}$$

where the basis is the interfacial area of the X phase in the total holdup, V_k, of the kth cell. Previously, a variety of situations were considered for the steady-state calculations, including those with non-uniform axial holdup and mixing of the phases and linear and non-linear equilibrium to quadratic order as

$$c^*_{x,k} = q' + mc_y + bc_y^2 \tag{2}$$

Here, methods of calculating the frequency-response characteristics of the same process based upon the backflow cell model are developed. The frequency-response technique is important as a means of identifying mixing-parameter models that apply to convective flow processes. Also, the dynamics and frequency-response characteristics of these processes are important with respect to the automatic control of them. Advanced control techniques involving feedforward and adaptive control require more sophisticated models of these processes.

Studies (*2*,*3*) of the dynamics of two-phase mass-transfer processes are ordinarily based upon the assumption of ideal plug flow in both phases. For linear equilibrium, analytical solutions are obtainable. However, if imperfect axial mixing is considered, the analysis becomes much more complicated. To date, no work is available that treats the frequency response for this case, except analyses (*2*,*4*) that are based upon a series of cells with no backflow terms. Frequency-response comparisons of the serial cell model with experimental data have been made by Gray and Prados (*2*) for a packed absorber and by Doninger

Downloaded At: 14:42 25 January 2011

and Stevens (4) for a packed extractor. Both studies indicate that more sophisticated models are required to describe accurately the interaction of mixing and mass transfer in the systems.

It is the purpose of this work to describe techniques for determining the frequency-response characteristics of the backflow cell model. These techniques are closely related to the methods of analysis and matrix techniques for computation outlined in the previous article (1). Here, the matrix techniques are based upon complex arithmetic procedures that are easily handled by most digital computers of the present day. The applicability of the backflow cell model is evaluated with respect to experimentally determined frequency-response characteristics of CO_2 absorption from air to water in a 6-in. diam packed column packed with ½-in. Intalox saddles and operating as a bubble-type column.

BACKFLOW CELL MODEL TECHNIQUES

Downloaded At: 14:42 25 January 2011

The set of dynamic equations for the backflow cell model are obtained by writing the dynamic solute material balance equations. One equation results for each cell of the X and Y phase. Each balance is formulated by equating the rate of accumulation of the solute in the cell to the net rate of input at any time. The net rate of input is the difference between the rates of input and output due to the mass transfer of solute between phases and by flow into and out of each cell. At steady state, the rate of accumulation or net rate of input is zero for each cell. This gives the set of algebraic equations treated in the previous paper (1) under the assumption of constant net flow rates, F_x and F_y, through the column between inlet and outlet points. As before, we will consider that the X-phase feed with solute concentration c_x^0 is introduced to the mth cell and that the Y-phase feed with solute concentration c_y^0 is introduced to the nth cell. These feed cells (m and n) are again assumed to be of negligible volume, which results in zero accumulation and mass transfer between phases. The density of the phase in each cell is assumed to be invariant with time. Thus, the rate of accumulation of solute in a cell is defined as the rate of change of the solute concentration times the holdup or volume of the particular phase in the cell.

With the foregoing considerations, typical dynamic solute material balance equations for the kth cell in the midsection are as follows:

$$V_{x,k}Dc_{x,k} = F_{x,k} \quad \text{and} \quad V_{y,k}Dc_{y,k} = F_{y,k} \tag{3}$$

where

$$F_{x,k} = (F_x + f_{x,k})c_{x,k-1} - (F_x + f_{x,k} + f_{x,k+1})c_{x,k} + f_{x,k+1}c_{x,k+1} - q_k \quad (4)$$

$$F_{y,k} = (F_y + f_{y,k})c_{y,k+1} - (F_y + f_{y,k} + f_{y,k-1})c_{y,k} + f_{y,k-1}c_{y,k-1} + q_k \quad (5)$$

These equations are of the same form in the end sections except

$$F_x = 0 \quad \text{for} \quad k < m \qquad \text{and} \qquad F_y = 0 \quad \text{for} \quad k > n$$

Equations (4) and (5) define the net rate of input functions, $F_{x,k}$ and $F_{y,k}$, which are zero at steady state as noted above. Again, it is convenient to subscript the backflow rates and volumes relative to each cell to allow for mixing and holdup variations along the axis of the system.

Previously it was convenient, at steady state, to divide the equations through by $F_x c_x^0$ and define dimensionless concentration ratios based upon the steady inlet X-phase composition. Now, however, the inlet feed compositions c_x^0 and c_y^0 are considered to vary sinusoidally with time about steady or constant values, $\bar{c}_x^0$ and $\bar{c}_y^0$, as follows:

$$c_x^0(t) = \bar{c}_x^0 + \Delta c_x^0 \sin \omega t, \qquad \text{and} \qquad c_y^0(t) = \bar{c}_y^0 + \Delta c_y^0 \sin \omega t \quad (6)$$

These input or forcing-function variations are restricted on a basis of one at time, although the methods would apply to simultaneous sinusoidal variations in each feed composition. With respect to the experimental determination of the frequency-response characteristics, the choice of forcing function depends upon how easy it is to manipulate each feed composition.

Now, the method of frequency-response analysis, which is based upon small input perturbations, $\Delta c_x^0 \sin \omega t$ and $\Delta c_y^0 \sin \omega t$, requires a set of linear differential equations. It is also convenient to write these in terms of deviation variables such that the constant or steady part of each equation vanishes. This part of the solution is assumed to be known from prior steady-state calculations (*1*). Thus the response variables or compositions may be expressed as functions of time by

$$c_x(t) = \bar{c}_x + \Delta c_x \qquad \text{and} \qquad c_y(t) = \bar{c}_y + \Delta c_y \quad (7)$$

The deviation compositions, Δc_x and Δc_y, vary sinusoidally with time. The method of linearizing the differential equations rests upon the same basis as the Newton–Raphson method of linearizing the steady-state equations as discussed in the previous paper (*1*). Each function

Downloaded At: 14:42 25 January 2011

of time in the composition variables is expanded as a Taylor's series about the steady-state compositions. Only first-order or linear terms are retained in terms of the deviation variables. Thus, the net rate-of-input functions are approximated by

$$F_{x,k} = \bar{F}_{x,k} + \sum_{j=1}^{n} \left(\frac{\partial}{\partial c_{x,j}} + \frac{\partial}{\partial c_{y,j}} \right) F_{x,k} \tag{8}$$

and similarly for $F_{y,k}$. But, $\bar{F}_{x,k} = \bar{F}_{y,k} = 0$, since they are evaluated at constant steady-state conditions. After the partials are evaluated and the substitution made into Eq. (3), the linearized dynamic equations result in terms of the deviation composition variables.

In order to facilitate the analysis, it is convenient to define generalized dimensionless deviation concentrations based upon $B = |\Delta c_x^0| + |\Delta c_y^0|$ as follows:

$$X = \frac{\Delta c_x}{B} \qquad Y = \frac{m \Delta c_y}{B} \qquad X^0 = \frac{\Delta c_x^0}{B} \qquad Y^0 = \frac{\Delta c_y^0}{B} \tag{9}$$

In this way, we may write the typical kth-cell dynamic equations as

$$\begin{aligned} \rho_{x,k} D X_k &= (p_x + \beta_{x,k}) X_{k-1} - (p_x + \beta_{x,k} + \beta_{x,k+1} + \alpha_k) X_k \\ &\quad + \alpha_k (1 + 2\chi) Y_k + \beta_{x,k+1} X_{k+1} \\ \rho_{y,k} D Y_k &= \beta_{y,k-1} Y_{k-1} - [p_y + \beta_{y,k} + \beta_{y,k-1} + \lambda \alpha_k (1 + 2\chi)] Y_k \\ &\quad + \lambda \alpha_k X_k + (p_y + \beta_{y,k}) Y_{k+1} \end{aligned} \tag{10}$$

where $p_x = 0, 1, 1$ and $p_y = 1, 1, 0$ in the regions of the cell model given by $(1 \leq k < m)$, $(m \leq k \leq n)$, and $(n < k \leq N)$, respectively. Also, for $k = m = n$, set $\alpha_k = 0$ and replace $p_x X_{m-1}$ by X^0 and $p_y Y_{n+1}$ by Y^0.

For a stable system of time-dependent linear differential equations, the frequency-response character is defined by the steady-state oscillatory response for steady sinusoidal forcing. Here, the oscillatory responses are the variations in the compositions produced after a steady sinusoidal change in one of the inlet feed compositions has been imposed at a certain frequency. The usual characteristics that are of interest for process-control purposes are the amplitude ratio and phase angle of an outlet response with respect to the sinusoidal input function. These are included in the particular or steady oscillatory solution profiles for $(1 \leq k \leq N)$ in the form

$$X_k(t) = |X_k| \sin(\omega t + \angle X_k) \quad \text{and} \quad Y_k(t) = |Y_k| \sin(\omega t + \angle Y_k) \tag{11}$$

Downloaded At: 14:42 25 January 2011

Here, $|X_k|$ and $|Y_k|$ are the gain factors and $\angle X_k$ and $\angle Y_k$ are the phase angles for the kth cell relative to either a unit sinusoidal change in the inlet X-phase feed composition, $X^0 = \sin \omega t$, or the Y-phase feed composition, $Y^0 = \sin \omega t$. It is convenient to use, as the test input function, a unit sinusoidal function with unit amplitude and zero phase. The gain factors and phase angles are functions of the frequency ω. A plot of the gain and phase characteristics versus frequency is the well known Bode type of plot. Methods of design of automatic control systems in the frequency domain are based on this type of plot.

The combination of gain and phase for a cell as a function of frequency may be represented as a phasor, $X_k(j\omega)$ or $Y_k(j\omega)$, in complex form with real and imaginary parts as

$$X_k(j\omega) = |X_k|\, e^{j\angle X_k} = X_{k,\mathrm{R}} + jX_{k,\mathrm{I}}$$

and (12)

$$Y_k(j\omega) = |Y_k|\, e^{j\angle Y_k} = Y_{k,\mathrm{R}} + jY_{k,\mathrm{I}}$$

With these forms, steady-state oscillatory responses in Eq. (11) are equivalent to

$$X_k(t) = \mathrm{Im}[X_k(j\omega)\, e^{j\omega t}] \quad \text{and} \quad Y_k(t) = \mathrm{Im}[Y_k(j\omega)\, e^{j\omega t}] \tag{13}$$

where Im means "the imaginary part of." These responses are substituted into the set of linearized differential equations, and since the differentiation, D, and Im operations commute, the term $e^{j\omega t}$ appears in all terms including X^0 and/or Y^0 and may be eliminated. This leaves a set of complex algebraic equations in the same form as Eqs. (10), but with the D operator replaced by $j\omega$ and X_k and Y_k replaced by phasors, $X_k(j\omega)$ and $Y_k(j\omega)$, respectively. This set of equations may be represented as a quidiagonal matrix system in the same manner as for the steady-state methods of solution discussed previously (*1*). Thus,

$$\tilde{A}\tilde{U} = \tilde{R} \tag{14}$$

where the phasor vector is the column matrix,

$$\tilde{U} = \mathrm{Col}\{X_1, Y_1, X_2, Y_2, \ldots, Y_N\}$$

and the input or forcing-function vector is the column matrix,

$$\tilde{R} = \mathrm{Col}\{r_{x,1}; r_{y,1}; r_{x,2}; \ldots; r_{y,N}\}$$

The quidiagonal-coefficient $\tilde{A}$ matrix is specified as before (*1*) with diagonals designated from left to right with elements a, b, c, d, and e,

Downloaded At: 14:42 25 January 2011

respectively. The major diagonal is along the diagonal of "c" elements. The elements along a diagonal alternate as, for example,

$$\{c_{x,1}\,;\, c_{y,1}\,;\, c_{x,2}\,;\, c_{y,2}\,;\, \ldots\,;\, c_{y,N}\}$$

The elements are defined as follows for $(1 \leq k \leq N)$:

$$\begin{aligned}
a_{x,k} &= (p_x + \beta_{x,k}) & a_{y,k} &= \beta_{y,k-1} \\
b_{x,k} &= 0 & b_{y,k} &= \lambda\alpha_k \\
c_{x,k} &= -[(p_x + \beta_{x,k} + \beta_{x,k+1} + \alpha_k) + j\omega\rho_{x,k}] & c_{y,k} &= -[p_y + \beta_{y,k} + \beta_{y,k-1} + \lambda\alpha_k(1 + 2\chi) + j\omega\rho_{y,k}] \\
d_{x,k} &= \alpha_k(1 + 2\chi) & d_{y,k} &= 0 \\
e_{x,k} &= \beta_{x,k+1} & e_{y,k} &= (p_y + \beta_{y,k})
\end{aligned} \tag{15}$$

As before, the exceptions to these occur at the end and feed cells where $a_{x,N} = e_{y,N} = 0$. Also, zero values are assigned to $\beta_{x,1}$; $\beta_{y,0}$; $\beta_{x,N+1}$; $\beta_{y,N}$; α_m; α_n; $\rho_{x,m}$; and $\rho_{y,n}$ because of the end conditions and the negligible holdup for the feed cells.

The solution of Eq. (14) for the phasor vector, $\tilde{U}(j\omega)$, yields the frequency-response characteristics depending upon where the sinusoidal forcing function is introduced. If a sinusoidal change in Δc_x^0 is considered, then $\Delta c_y^0 = 0$ and $X^0 = 1$, which means that all of the elements of the $\tilde{R}$ vector are zero except one, which is $r_{x,m} = -1$. Similarly, for a sinusoidal change Δc_y^0 in the Y-phase feed composition, $\Delta c_x^0 = 0$ and $Y^0 = 1$, and all elements of $\tilde{R}$ are zero except the one relative to that feed cell, namely, $r_{y,n} = -1$. The form of B in Eq. (9) ensures division of the gains by the amplitude of the particular input wave that is acting. The solution of the quidiagonal matrix system of equations for each assumed frequency ω is efficiently carried out by the Gaussian elimination procedure with the recursive relationships given by Conte and Dames (*5*). These were coded in complex arithmetic. The digital computation gives the phasor vector, $\tilde{U}(j\omega)$, as a set of complex numbers at each frequency. Thus the complete profile of phasors is obtained. This indicates the gain and phase of the sinusoidal wave as it travels from cell to cell in both phases due to both flow and the interaction of interphase mass transfer. The amplitude ratio for any particular cell k at a given frequency ω is defined as the gain factor $|X_k(\omega)|$ at the frequency divided by the gain factor $|X_k(0)|$ at zero frequency. Further details of the derivation and calculation of theoretical frequency-response characteristics based upon the backflow cell model are given by McSwain (*6*).

Downloaded At: 14:42 25 January 2011

The method of digital complex arithmetic calculation avoids the tedious reduction of such a topological system as the cell model by conventional methods of block-diagram algebra or signal-flow diagram methods (7). To perform these algebraic manipulations for a large number of cells would be very difficult. However, once numerical values are assigned to the constants and the frequency, recursive manipulations in complex arithmetic could be coded. This program would amount to the same procedure as the solution method noted above for the matrix system of equations.

The techniques, as outlined here, allow frequency-response characteristics, which have not been obtained previously, to be obtained for the cell model with backflow and interphase mass transfer. Although the techniques apply to the backflow cell model, the frequency-response characteristics are approximations to those of the continuous two-phase "eddy diffusion" or dispersion model when the "phi" number ϕ for each phase is equal to the equivalent Peclet number N_{Pe} of the dispersion model. It was previously shown (1) that the steady-state profiles of the backflow cell model converge to those of the dispersion model on the order of N^{-2} as the number N of cells increases at constant "phi" numbers ϕ_x and ϕ_y for the phases. No frequency-response results for the dispersion model are presently available for comparison. In general, the convergence would hold because of the spacewise finite difference character of the backflow cell model, although the rate of convergence may vary somewhat, mainly because of problems with the rounding off of numbers. Again as before for the steady state profiles, the continuous frequency-response profiles at a given frequency for the dispersion model would best be approximated by the cell model with $\phi = N_{Pe}$ values when smooth curves are drawn through the average values of adjacent cells assigned to the position between these cells.

Downloaded At: 14:42 25 January 2011

EXPERIMENTAL APPARATUS AND PROCEDURE

The change with time in the concentration of tracer in air at the top of a packed column was observed after a step change was made in the tracer content of the inlet air. Absorption of the tracer gas occurred into water flowing downward countercurrently to the air flow. The column was operated in the bubble mode—that is, with air, the dispersed phase, bubbling through the water with its interface at the top

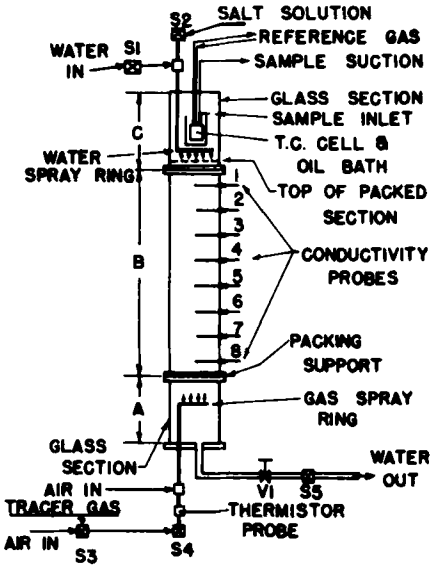

FIG. 2. Schematic diagram of packed column.

of the packing. A schematic diagram of the packed absorption column is shown by Fig. 2. The column consisted of sections A, B, and C flanged together. Section B is made of 6-in. i.d. aluminum pipe and sections A and C are nominal 6-in. diam glass Pyrex pipe. The column was filled to a height of 74.8 in. with ½-in. Intalox saddles. The packing-support plate was made by drilling ½-in. holes in a ¼-in.-thick aluminum plate to give about 20% free area.

Water was supplied to the top of the column through a spray-ring coil of ½-in. copper tubing with $\frac{3}{64}$-in. diam spray holes. The water level was adjusted by means of valve V1 on the outlet stream. The level was maintained as close as possible to a mark between the packing and the spray ring. The holdup of the water phase was determined by weighing the water drained from the column after the solenoid valves were closed. These valves were S1 on the inlet water, S4 on the inlet air, and S5 on the outlet water stream. The water flow rate was determined by weighing a timed sample of the effluent during a run. The air-distributor coil was made in the same manner as the water-spray ring. The tracer gas indicated was either argon or carbon dioxide from a standard compressed-gas cylinder. The tracer could be

Downloaded At: 14:42 25 January 2011

admitted to the inlet air stream by means of solonoid valve S3. The flow rates of the air and tracer gases were determined by rotameters in the lines.

The concentration of tracer gas in the outlet air streams was monitored by means of a Gow-Mac Type 9677 thermal-conductivity cell. The elements of this cell were type G-112 thermistors, one for the sample gas and one for the reference gas. These were joined in the usual manner with standard resistors as a Wheatstone bridge connected to a dc power supply. The output voltage signal, which varied with the thermal conductivity of the sample gas, was amplified and recorded by a two-channel oscillographic recorder. The thermal-conductivity cell was immersed in a small oil bath with heater. This assembly was placed directly inside the top glass section C of the column above the spray ring. The sample inlet extended perpendicular into the flow of gas around the oil bath. Lines of ¼-in. polyethylene tubing were brought from the sample and reference sides of the cell to vacuum. Each line was connected first to a needle valve and small rotameter and then to a capacitance tank attached to a vibrating-diaphragm suction pump. The needle valves and rotameters allowed the sample and reference gas flows to be adjusted to about the same rate. Fine adjustments of the balance of the Wheatstone bridge were made with variable resistors. Prior to the use of the thermal-conductivity cell in the column, its voltage output signal was found to vary linearly with tracer-gas concentration at a constant temperature. These tests were made by sampling the exhaust of a mixing chamber into which air and tracer gas were metered at constant flow rates.

Downloaded At: 14:42 25 January 2011

After allowing the column to come to equilibrium at the desired air and water flow rates and with the sample and reference flows adjusted, the solenoid valve S3 was opened to allow sudden and continuous injection (a step-up change) of the tracer gas into the inlet air stream. During the time of tracer-gas injection, the change in thermal conductivity of the effluent gas stream was recorded. The set of step-up response tracings recorded for carbon-dioxide injection is shown by Fig. 3. The response traces were staggered one above the other to prepare this figure. The chart lines were photographically filtered out to leave only the black tracings on the heat-sensitive paper. The step-up responses for argon were much faster because of negligible absorption. Further details of the experimental study and preliminary results are given by McSwain (*6*).

The space time, τ_L, for the liquid (water) phase was determined as

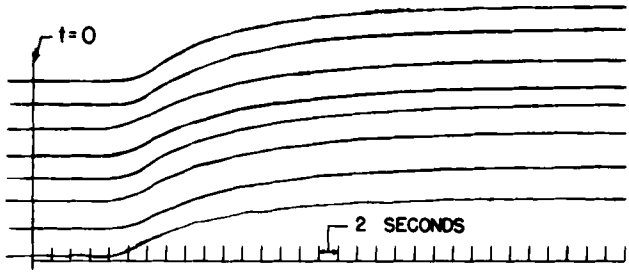

FIG. 3. Experimental outlet-gas responses to step input of carbon dioxide in the inlet gas. Shown, starting from the top of the figure, are Runs 1A, 1B, 5A, 5B, 2, 6, 7, and 4B-CO_2.

the ratio of measured holdup to measured flow rate for each run. The space time, τ_G, for the gas (air) phase was taken to be the ratio of gas-phase holdup to flow rate. The gas-phase holdup was determined as the difference between the total void volume and the liquid-phase holdup. The column space times are indicated for the different runs in Table 1. The gas (air) flow rates for the runs indicated by Table 1

TABLE 1

Run no.	Column temp, °F	τ_L, sec	τ_G, sec	$N_{Re,L}$	t_D, sec	$N_{Pe,G}$	$N_{Pe,L}$	N_{ox}
Argon tracer runs								
2	86	∞	6.4	0	2.8	35.7		
3	88	50	7.4	1170	3.4	17.3		
4A	88	136	6.5	435	3.3	27.8		
4B	88	136	6.5	435	3.2	41.0		
5	88	131	6.5	452	3.1	46.8		
6A	88	165	6.6	362	3.0	41.0		
6B	88	165	6.6	362	3.3	34.2		
7	81	∞	7.3	0	3.4	26.4		
Carbon dioxide absorption runs								
1A	79	222	6.6	267	5.0	35.1	21.9	25.5
1B	79	222	6.6	267	5.0	35.1	21.9	25.5
2	83	119	6.9	490	4.2	29.7	34.9	14.0
4B	84	50	7.5	1167	3.2	18.5	86.4	6.2
5A	86	151	6.3	399	4.4	32.0	29.3	17.1
5B	86	151	6.3	399	4.4	32.0	29.3	17.1
7	89	64	6.9	946	5.0	21.9	65.5	7.6

Downloaded At: 14:42 25 January 2011

were constant at 12.5×10^{-5} lb-moles/sec. Also, the mid-point column pressure was 15.8 ± 0.1 psia. The column temperature indicated was measured midway in the packed section by means of a glass thermometer.

NUMERICAL FOURIER TRANSFORMATION

The experimental frequency-response characteristics relative to each step response run were obtained by numerical Fourier transformation of the pulse function, $p(t)$, obtained as

$$p(t) = 1 - v(t) \tag{16}$$

Here, $v(t)$ is the normalized step response based on a total pen deflection of 0 to 1.0 for each recording. Now, $p(t)$ is Fourier transformable, whereas $v(t)$ is not. The Fourier transform, in terms of its real and imaginary parts at a given frequency ω, may be calculated as

$$P(j\omega) = \int_0^{t_c} p(t) \cos \omega t \, dt + j \int_0^{t_c} p(t) \sin \omega t \, dt \tag{17}$$

where t_c is the record length. This is taken to be slightly larger than the time for the step response to reach the final steady state in a practical sense. Numerical values of $P(j\omega)$ were obtained for each step-response curve for a range of assumed values of the frequency. The integration indicated by Eq. (17) was carried out using Filon's (*8*) method of the Simpson's rule type of integration. A time increment of 0.5 sec was used in digitizing the step-response curves.

For each calculated value of $P(j\omega)$, the transfer-function characteristics can be obtained as

$$G_y(j\omega) = 1 - j\omega P(j\omega) \tag{18}$$

From the real and imaginary parts of this function, the amplitude ratio or unit gain factor $|G_y|$ and the phase angle $\angle G_y$ were calculated at each assumed frequency. These had to be corrected for the measurement time lag due to the thermal-conductivity cell. The step response for the thermal-conductivity cell by itself was measured by suddenly inserting the sample suction port into an atmosphere of carbon dioxide and air. The step response of the instrument by itself could be predicted to a least-mean-square fit by two first order transfer functions in series with equal time constants of $T_m = 1.09$ sec. These values were used to correct the calculated gains and phase angles for the measurement dynamics.

The calculated values of $|G_y|$ and $\angle G_y$, after correction for the

Downloaded At: 14:42 25 January 2011

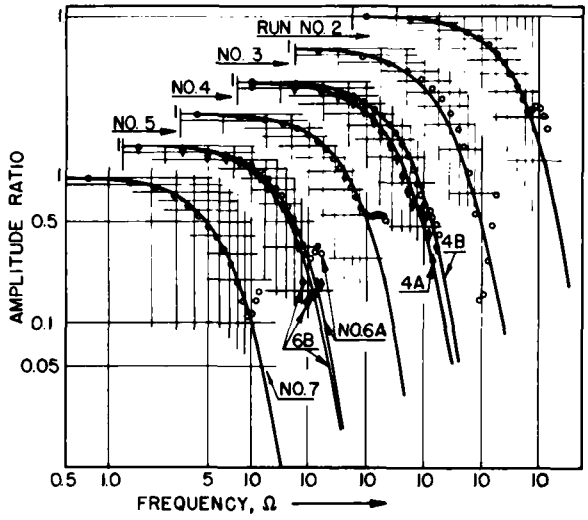

FIG. 4. Argon outlet-gas amplitude frequency responses without monitoring and transport lags. Points calculated from experimental argon step-up responses and solid lines from the backflow cell (8-82-11) model with best betas.

Downloaded At: 14:42 25 January 2011

measurement and sampling time lags, are shown as the points in Figs. 4 and 5 for the argon runs and in Figs. 6, 7, 9, and 10 for the carbon dioxide runs. The curves on these figures are those calculated for the backflow cell model. The frequency base is the reduced frequency, $\Omega = \omega\tau_G$, defined as the actual frequency times the space time τ_G of gas in the column. In order to display all of the data points and fits in a compact form without crowding, they were staggered along the abscissa in Figs. 4, 5, 9, and 10. The frequency base for each successive curve and group of points from left to right may be obtained by successively shifting the scale on the left so that the lines at $\Omega = 5$ or 10 are aligned. The curves on Figs. 4 and 5 for argon are staggered vertically as well. However, the grid lines given allow one to count from unit amplitude ratio or zero phase-lag angle.

The calculated frequency-response characteristics start to become erratic beginning at about $\Omega = 10$ for argon and after $\Omega = 5$ for carbon dioxide. The responses for argon are sharper and thus resolution to higher frequencies is obtained. The erratic behavior at high frequencies is due to a number of causes, including the lower frequency content of the step-response data and numerical difficulties associated with numerical Fourier-transformation techniques. The use of a step

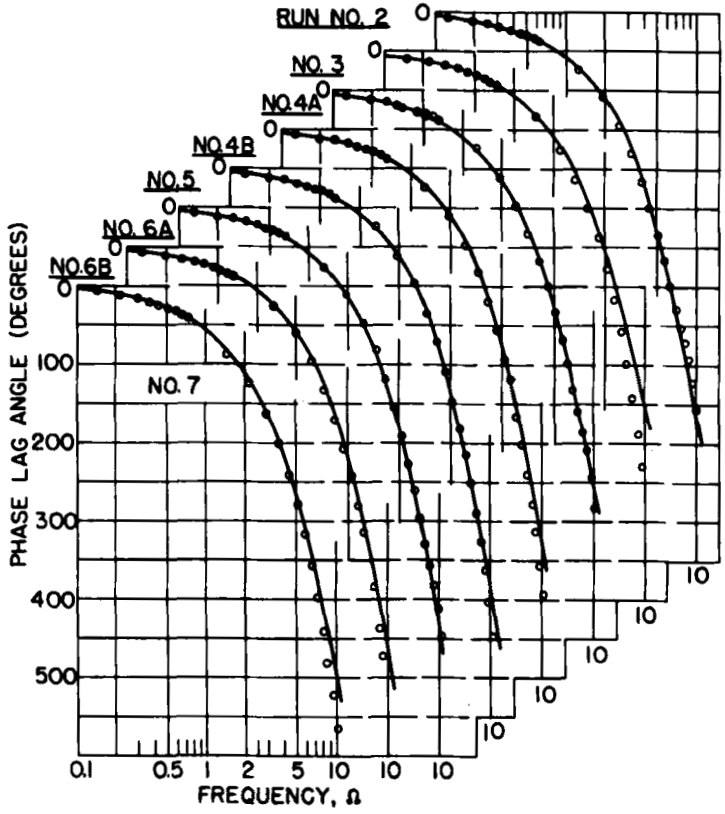

FIG. 5. Argon outlet-gas phase angle frequency responses without monitoring and transport lags. Points calculated from experimental argon step-up responses and solid lines from the backflow cell (8-82-11) model with best betas.

type of input function became necessary because of the unavailability of the necessary equipment required to maintain sinusoidal variations of the carbon-dioxide content of the feed gas. Any pulse type of input has greater high frequency content than the step function. However, unless the pulse duration is sufficiently long, not enough tracer can be introduced to allow for absorption and obtain a good pulse response at the top.

It should be stressed that frequency-response data obtained in the classical manner with a sinusoidal input at each frequency would begin to become erratic in the high-frequency region also. This is associated

Downloaded At: 14:42 25 January 2011

with difficulties in accurately reading the amplitude ratio and phase shift at the higher frequencies, where the highly attenuated sinusoidal response is distorted by noise. The wave signals would have to be averaged as with a wave analyzer to obtain more reliable results. This would be similar to analyzing a number of step-response curves and averaging the results. For example, Argon Runs 6A and 6B and Carbon Dioxide Runs 5A and 5B, by themselves, give erratic results at the higher frequencies. If they are averaged, however, much smoother variations are obtained.

For practical purposes having to do with simulation and process control the results obtained here are useful in that the predominant time-lag and delay characteristics are defined considerably past the critical frequency. Other time lags in any control loop would further damp the signal character and shift the significance of the column characteristics to even lower frequencies.

The results given by Gray and Prados (*2*) indicate that difficulties with the classical frequency-reponse technique are also experienced at high frequencies. In their case, the frequency-response character of a mock-up section including only the end sections of the column was extracted to obtain the character of the packed section. Their data for a gas rate of 1 lb mole/hr-ft^2 corresponds to a gas-phase residence time of about $\tau_G = 0.5$ min. Thus, their highest recorded frequency of 4 cycles/min corresponds to a reduced frequency of about $\Omega = 12.5$ rad. At this frequency and at zero water flow, the following amplitude ratios are indicated: 0.03 for the overall column; 0.06 for the mock-up section; and 0.5 is calculated for the packed section. Thus, the dynamics of the measurement and mock-up sections are predominant. At the higher frequencies, the amplitude ratios are so low already that good definition of those for the packed section cannot be obtained. In our case, the frequency-response characteristics of the complete column are obtained. However, the void space in the end sections is at a minimum and the results are more characteristic of the packed section than those by Gray and Prados (*2*). Their calculated amplitude-ratio curves for the packed section flatten out at the higher frequencies. Our results do not indicate this flattening, and much lower amplitude ratios are observed.

BACKFLOW CELL MODEL SIMULATION

Brittain and Woodburn (*9*) obtained steady-state experimental gas-(air) phase carbon dioxide concentration profiles for a trickle bed.

Downloaded At: 14:42 25 January 2011

They compared these with those predicted by a model considering the gas with axial mixing and the liquid (water) in plug flow. Here, the liquid-phase mixing in the bubble column is more severe. Also, the absorption of carbon dioxide into water is controlled by the liquid-phase resistance. Thus, the influence of mixing in the liquid phase will be important. From the standpoint of fitting the backflow cell model with a given number of cells, we have several parameters that are not easily specified; namely, the backflow ratios β_x and β_y and the number of transfer units N_{ox}. Alternatively to β_x and β_y, the phi numbers ϕ_x and ϕ_y may be specified. For a large number of cells these may be noted as $N_{Pe,x}$ and $N_{Pe,y}$, respectively, on the basis of the continuous-dispersion model.

The backflow cell model of the column was considered in three sections with 11 cells for the region from the top of the packing to the water level, 82 cells for the packing, and 8 cells for the region from the bottom of the packing to the air-injection ring. This model is termed the (11-82-8) BCM (for backflow cell model). The positive z direction is considered to be the direction of flow of the water phase. Thus, the X phase is the water phase and the Y phase is the gas phase. Also, with respect to Fig. 1, the feed cells are at the respective ends of the column. The assignment of the X phase to the water phase means that N_{ox} is identical to N_{oL}, the number of liquid-phase mass-transfer units. This is appropriate because of the controlling factor due to the liquid phase for the carbon-dioxide absorption.

The assignment of three regions to the model is necessary because of the different phase holdups in the regions per unit length. The void volumes of the three regions—namely, the top, packing, and bottom regions—were determined to be 0.104, 0.788, and 0.074 ft^3, respectively, with respective lengths of 6.4, 74.8, and 4.5 in. The void volumes of all cells in the column were made approximately equal, and this resulted in the (11-82-8) configuration. Those in the top and bottom sections were slightly off because of the requirement of an integer number of cells in each case. The number of cells is sufficiently high so that with $\phi = N_{Pe}$ for each phase a very good approximation to the continuous-dispersion model may be expected. This is indicated by the comparisons of the moments of the impulse response of the two models for single-phase flow made by Roemer and Durbin (*10*). For example, with 100 cells the percent deviations are about 0.1 in the variances and 1.0 in the central skew moments for $N_{Pe} = 40.0$. Since the moments are related to the curvature and form of the amplitude-ratio and

Downloaded At: 14:42 25 January 2011

phase-angle curves, quite good correspondence is to be expected here for the number of cells chosen.

The assignment of the holdups to the different regions was made by first assuming that the air-phase holdup or accumulation factor $\rho_{y,k}$ in Eqs. (10) was given by $\rho_{y,k} = (P_k V_{y,k})/(F_y RT)$ where $V_{y,k}$ and F_y are measured at the same conditions and P_k is the pressure at the mid-point of the cell. The pressure variation was taken to be a linear function of the distance along the column such that the total pressure drop equaled the friction drop of 2 psig that was noted. The variation of the liquid- (water) phase holdup is mainly influenced by the presence of packing since the column was operated as a bubble column. The liquid-phase holdup $V_{x,k}$ for a cell in the packing was taken to be 0.644 times that of one not in the packing section.

The "phi" number ϕ_i of the ith phase in any section or region R of the column with length ℓ is defined relative to the packed section as

$$\phi_i = \frac{2N_R L_P}{\ell(p_i + 2\beta_i)} \tag{19}$$

This applies for uniform Peclet number (or β's) along the axis of the section. It is assumed that the axial dispersion or eddy diffusion coefficient D_i for each phase is the same in all three sections. Then, the ratio of Peclet numbers (or ϕ's) in any two sections is proportional to the ratios of the product of velocity times length. For the gas phase, a logical assumption is that its velocity is uniform and thus β or N_{Pe} is uniform along the axis. However, the relative velocity of the liquid phase in the packed section is considered to be inversely proportional to the void fraction, which is 0.644 for the ½-in. Intalox saddles. Under these assumptions, liquid-phase Peclet numbers or ϕ values of 0.055 and 0.039 times those of the packed section result, respectively, for the top and bottom sections.

The axial-mixing characteristics of the water phase in this same column at the same gas-flow rate were investigated (*6*). Salt solution was pulse injected at the top of the column and the electrical conductivity of the water phase was monitored at six points along the packed section. The responses were analyzed by transient response and moments techniques (*10*) to obtain the best fit of the single-phase backflow cell model in the time domain. The variation of the liquid-phase eddy diffusivity with water-flow rate was found to be approximately constant. This confirmed the validity of specifying the liquid-

Downloaded At: 14:42 25 January 2011

phase mixing parameters for the different sections on the basis of the assumption of uniform eddy diffusivity along the axis.

The single-phase (8-82-11) model was also used to fit the argon step-response curves by varying the mixing and time delay parameters (*6*). The parameters for the best fits in the sense of least-mean-square deviation between experimental and model step responses are indicated in Table 1. The overall gas-phase Peclet number $N_{Pe,G}$ is based upon the packing section. The results indicate that this is relatively insensitive to the overall liquid-phase Reynolds number $N_{Re,L}$ or velocity except at the high flow rates, where a decrease is noted. The results are consistent with the assumption of uniform gas-phase eddy diffusivity, since the changes in liquid-phase velocities in the column are not too severe. We consider the ratio of the velocity in an end section to that in the packing to be equal to $\epsilon = 0.644$. Thus, for this variation, the assumption of uniform gas-phase mixing is good.

Downloaded At: 14:42 25 January 2011

COMPARISON OF FREQUENCY-RESPONSE RESULTS

In order to test the validity and usefulness of the numerical Fourier transformation techniques, the results for argon as a tracer were compared to the theoretical predictions based upon the backflow cell model. First, the argon step-response curves were Fourier transformed and plotted as the points in Figs. 4 and 5, as noted earlier. Then, the outlet-gas amplitude ratio and phase angle relative to a sinusoidal variation in the inlet gas-phase concentration to the (8-82-11) backflow cell model were computed according to the methods outlined above. The results are plotted as the solid lines in Figs. 4 and 5. These computations were made with the same values of N_{Pe} and deadtime t_D as obtained for the best fits in the time domain. The value of N_{ox} was taken to be zero so that no interaction occurred between the phases. Alternatively, the single-phase model could be used. The complex matrix equation is specified by a tridiagonal system in this case.

As shown by Figs. 4 and 5, the comparisons between the model and the experimentally derived frequency-response characteristics for the argon runs are very good for the frequency range less than $\Omega = 10$. At this frequency, the amplitude ratio is about 0.1 and the phase angle is about $-500°$. Thus, for practical control and simulation, the results are realistic and useful. The amplitude-ratio curves for Argon Runs Nos. 4A and 4B do not agree because of the different values of $N_{Pe,G}$ as determined from the time-domain analysis. However, each agrees with the experimentally derived points. This indicates that the fre-

quency-response techniques do indicate the degree of difference noted. Thus these frequency-response techniques would be useful in specifying system parameters. The degree of variation between Argon Runs Nos. 4A and 4B point out the difficulty of analyzing the faster-rising argon curves with the measurement lag present. The poorer fit for Argon Run No. 3 is due to the much higher water rate employed. It was observed that the water entrained very small air bubbles and carried them along for a short distance below the air input point. This would add another more macroscopic type of backflow, possibly over several cells in the model. Such an analysis was not made, and this run is included to show the effects of this type of phenomenon. The main characterization of the small-scale backmixing is satisfied by the value of $N_{Pe,G} = 17.3$ that was obtained.

The estimated values of $N_{Pe,G}$ from the argon runs and $N_{Pe,L}$ from the salt-tracer runs were plotted versus the liquid-phase Reynolds number (*6*). Smooth curves through the respective sets of data yielded the estimates of $N_{Pe,G}$ and $N_{Pe,L}$ as indicated in Table 1 for the carbon dioxide runs. The fact that the argon frequency-response characteristics could be predicted by the model with parameters specified by the best fit in the time domain led us to believe that the procedure could be reversed to analyze the carbon dioxide runs. There are no analytical solutions available for calculating the step response of the two-phase models. Thus, timewise integration is called for with a resulting increase in computer time for the more complex system and longer time records. The computational effort builds up rapidly with the number of cases with different parameters required to obtain the best fit of the response. Frequency-response calculations for the model need be made only at a selected number of frequencies to define the amplitude-ratio and phase-angle curves. This greatly reduces the computational effort.

The frequency-response analysis of the carbon dioxide runs was initiated by first computing the characteristics for different values of N_{ox} with the parameters relative to those for Carbon Dioxide Run No. 2 in Table 1. The slope of the equilibrium line required to specify λ was calculated from Henry's-law coefficients as given by Perry (*11*). The model results as shown by Figs. 6 and 7 indicate that $N_{ox} = 14$ gives the best fit of the experimental points for this run. Also, the agreement is quite realistic out to the frequency range $\Omega = 5$ to 10.

With respect to the frequency-response plots, it should be noted that the experimental points have been corrected for the monitoring lag specified by two first-order time constants of 1.09 sec in series and

Downloaded At: 14:42 25 January 2011

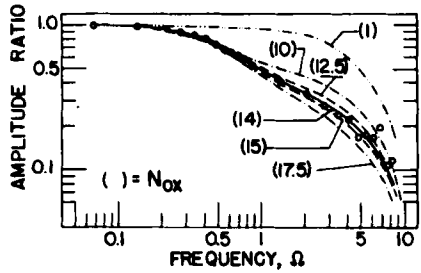

FIG. 6. Outlet-gas amplitude-ratio frequency response. Lines calculated from (11-82-8) BCM and points from Run 2-CO_2, excluding monitoring and transport lags.

a transport lag. The transport delay or dead time t_D was assumed to be the cumulative time for transport of the tracer gas from the point of injection to introduction into the column and then from the outlet gas above the water level through the sample tube to the thermistor sensing element of the conductivity cell. No consistently satisfactory method was available for independently estimating the dead time t_D. Thus, this may be regarded as another parameter to be specified from the data. The dead time does not affect the amplitude-ratio curves so that the estimate of N_{ox} is best achieved with respect to these curves. However, the dead time adds to the phase-lag angle a component that increases linearly with frequency.

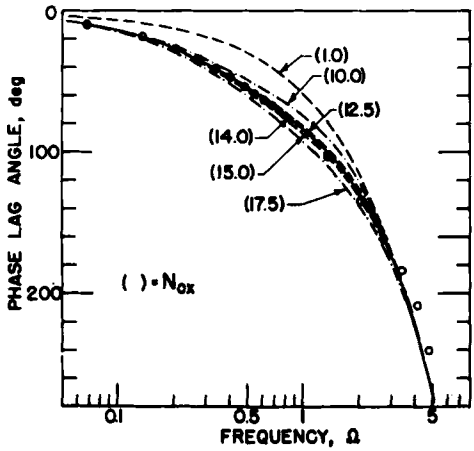

FIG. 7. Outlet-gas phase-angle frequency response. Lines calculated from (11-82-8) BCM and points from Run 2-CO_2, excluding monitoring and transport lags.

Downloaded At: 14:42 25 January 2011

For Carbon Dioxide Run No. 2 with $N_{ox} = 14$, the estimation of the dead time t_D was made by averaging the additional delay times required to make the theoretical phase-lag curve match the experimental phase-lag curve at frequencies of $\Omega = 1$, 2, and 3. The phase-lag angle due to this dead time of 4.2 sec was subtracted from each experimental point. These corrected points are the ones plotted in Fig. 5. The frequency range that was selected occurs in the rapidly changing part of the phase-lag curve. As indicated by Fig. 5, for the higher frequencies above $\Omega = 2$, the theoretical phase-lag curves are fairly independent of N_{ox}. Even with the dead time known beforehand, it would be more difficult to estimate the best value of N_{ox} using phase-lag curves such as displayed by Fig. 7. However, Fig. 7 indicates that a value of $N_{ox} = 14$ is consistent with model variations and the data.

The indication is that the phase lag of the model increases with frequency slightly more rapidly than the experimental data. It is believed that this is due to the loss of resolution with the numerical Fourier transformation techniques. In general for process control with negative feedback, good definition of frequency-response characteristics is required out to the critical frequency for which the phase lag is 180°. Thus, in this respect the model simulation of the absorption column with $N_{ox} = 14$ for Carbon Dioxide Run No. 2 is quite satisfactory.

The amplitude and phase-lag angle characteristics of the concentration X_{111} of carbon dioxide in the outlet liquid (water) phase of the (11-82-8) backflow cell model relative to sinusoidal variations in the inlet-gas-phase concentration were computed for the conditions of Run No. 2 with $N_{ox} = 14$. These characteristics are shown plotted versus frequency in Fig. 8. The reduced frequency basis $\Omega = \omega\tau_G$, as based upon the gas-phase space time, is retained so that more direct comparisons with the gas-phase characteristic curves may be made. Interestingly enough, the amplitude-ratio curve decreases only slightly faster than that for the gas out. However, the phase-lag curve shows a much slower increase with frequency than the gas-out curve. This is due to the coupling by mixing and mass transfer between the gas and liquid cells right after the gas inlet point. The net effect is to decrease the phase-lag angle.

The comparison of the data for the other carbon dioxide absorption runs was made under the assumption that the mass-transfer-rate factor ($k_{ox}a$) is constant for the bubble-column operation. Alternatively, this means that the product ($F_x N_{ox}$) is a constant. In this way,

Downloaded At: 14:42 25 January 2011

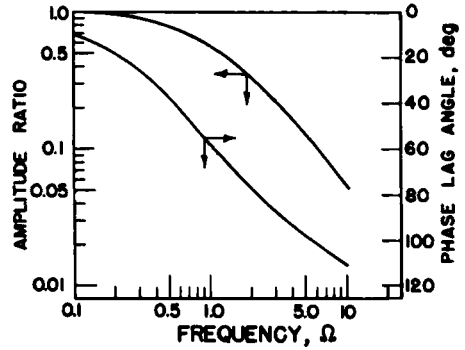

FIG. 8. Outlet-liquid frequency response characteristics. Calculated from (11-82-8) BCM with $N_{ox} = 14.0$.

N_{ox} for each run was estimated on the basis of the best value of $N_{ox} = 14$ for Carbon Dioxide Run No. 2. These values of N_{ox} are given in Table 1. Other parameters relative to the conditions of each run as given in this table were obtained in the same manner as indicated above for Run No. 2. For each run, the amplitude-ratio and phase-angle characteristics of the outlet gas of the (11-82-8) backflow cell model were computed. These are compared with those derived from the experimental data in Figures 9 and 10. Again, the experimental phase-lag points are those corrected for dead time in the same manner as noted for Run No. 2. The estimated dead time for each run is given in Table 1.

The frequency-response comparisons in Figs. 9 and 10 indicate that the assumption of constant $(k_{ox}a)$ with respect to water flow rate is a fairly good approximation. Some increase in N_{ox} for Carbon Dioxide

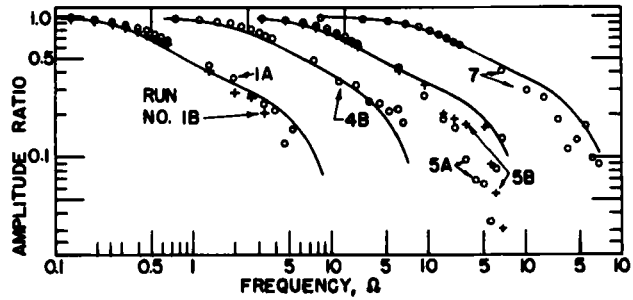

FIG. 9. Outlet-gas amplitude-ratio frequency responses for various carbon dioxide runs. Lines calculated from (11-82-8) BCM and points from experimental data, excluding monitoring and transport lags.

Downloaded At: 14:42 25 January 2011

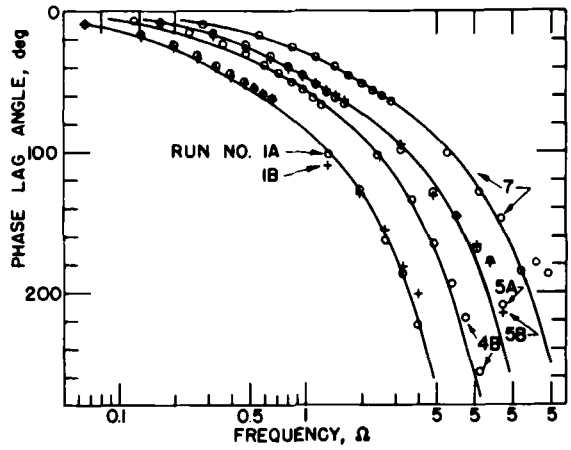

FIG. 10. Outlet-gas phase-angle frequency responses without monitoring and transport lags for the absorption of carbon dioxide by water. Solid lines are calculated from the (11-82-8) BCM and points from experimental data.

Runs Nos. 5 and 7 is indicated by the amplitude-ratio data. Before any correlation of N_{ox} is undertaken, further test data from pulse and sinusoidal responses should be analyzed. However, these results indicate that the backflow cell model can be used to simulate the system for different conditions with an adjustment of parameters.

CONCLUSION

The backflow-cell-model equations have been developed for the two-phase flow process with imperfect axial mixing and mass transfer of a single solute. Methods of solution for the frequency-response characteristics of this model have been developed and the techniques outlined for digital computation.

The frequency-response characteristics of the model have been compared to those obtained for the system of air and water in countercurrent flow in a packed bubble column with step injection of argon and carbon dioxide tracer gases. The model frequency-response characteristics, as determined with parameters specified by the best fit of the argon step responses, agreed closely with the experimentally derived frequency-response data. This served to indicate that the parameters necessary to specify the system with carbon-dioxide absorption could be estimated by these frequency-response techniques. By variation of the number of transfer units N_{ox}, the model and experimental

Downloaded At: 14:42 25 January 2011

amplitude-ratio curves can be brought into very good agreement for the range of frequencies of practical interest. The phase-lag–angle curves are not as reliable because of the influence of injection and sampling dead time. For variations in the liquid flow rate, the results of the study for this bubble column indicate that the backflow cell model is a useful dynamic model. Some adjustment in N_{ox} would be required as a function of liquid flow rate. The methods of calculating frequency-response characteristics from the step response appear to be useful for practical process-control analysis. This is doubly so, since the step response is more readily obtained than any other type of characteristic response without recourse to specialized and expensive equipment.

List of Symbols

$a, b, c, d, e, r,$	in form $a_{i,k}$; elements of quidiagonal coefficient $\tilde{A}$ matrix
a	interfacial area per unit volume of system, ft²/ft³
a_k	interfacial area per unit volume in the kth cell
A	cross-sectional area of column
$\tilde{A}$	quidiagonal coefficient matrix from combined X and Y equations
b	curvature of equilibrium line
c_i	concentration of solute in the ith phase, lb moles/ft³
c_i^0	inlet concentration of solute in the ith phase
D	derivative operator, d/dt
D_i	eddy diffusion coefficient for the ith phase, ft²/sec
$f_{i,k}$	backflow rate of the ith phase from the kth cell, ft³/sec
F_i	flow rate of ith phase, ft³/sec
k_{ox}	overall mass-transfer coefficient based on X phase, ft/sec
ℓ	actual length of any section of column, ft
L_p	actual length of packed section of column, ft
m	slope of equilibrium relationship; cell with X-phase feed
n	cell with Y-phase feed
N	total number of cells in system including those in the end sections
N_R	number of cells in a region R
$N_{Re,L}$	liquid-phase Reynolds number (average superficial velocity × nominal packing size)/kinematic viscosity

Downloaded At: 14:42 25 January 2011

N_{ox} number of transfer units, $k_{ox}\alpha L_p/F_x$

$N_{Pe,i}$ dimensionless Peclet number for the ith phase in any section $u_i\ell/D_i$

p_i coefficient element for net flow of the ith phase in a region, 1 if or 0 if not

q' intercept of equilibrium expression

q_k mass transfer between X and Y phases in kth cell, Eq. (1)

$r_{i,k}$ element of $\tilde{R}$ for ith phase and kth cell material balance

$\tilde{R}$ constant column vector from combined X and Y equations

t actual time, sec

t_D transport or dead time, sec

u_i linear velocity, ft/sec

$\tilde{U}$ alternating X and Y profile column phasor vector

V total volume of system

V_k volume of X and Y phases in kth cell

$V_{i,k}$ volume of ith phase in kth cell

X generalized solute concentration deviation in X phase

X^0 generalized solute concentration variation in X-phase feed

Y generalized solute concentration deviation in Y phase

Y^0 generalized solute concentration variation in Y-phase feed

z axial length dimension from X-phase input, ft

Greek Letters

α_k dimensionless rate constant for mass transfer in kth cell, $N_{ox}V_k/V$

$\beta_{i,k}$ backflow ratio from kth cell in ith phase, $f_{i,k}/F_i$

Δy deviation in arbitrary variable y from constant steady state

ϵ void fraction

λ dimensionless capacity ratio, mF_x/F_y

$\rho_{i,k}$ holdup rate constant for ith phase, $V_{i,k}/F_i$

τ space time

ϕ_i "phi" number for the ith phase, Eq. (19)

χ dimensionless curvature of equilibrium relation $(bc_x^0)/m^2$

ω actual frequency, rad/sec

Ω reduced frequency $\omega\tau_G$, dimensionless

Downloaded At: 14:42 25 January 2011

Subscripts

G	gas phase
i	phase, X or Y
I	imaginary part of
k	arbitrary cell
L	liquid phase
m	X-phase feed cell
n	Y-phase feed cell
R	real part of
x, y	X or Y phase

Superscripts

$-$	constant steady-state value
^{0}	feed condition
*	equilibrium

Downloaded At: 14:42 25 January 2011

Acknowledgments

Digital computations were performed by the Data Processing Center of the Texas Engineering Experiment Station. This support is greatly appreciated. The first author acknowledges fellowship assistance by the Dow Chemical Company.

REFERENCES

1. C. V. McSwain and L. D. Durbin, *Separation Sci.*, **1**, 677 (1966).
2. R. I. Gray and J. W. Prados, *A.I.Ch.E. J.*, **9**, 211 (1963).
3. J. C. Biery and D. R. Boylan, *Ind. Eng. Chem. Fundamentals*, **2**, 44 (1963).
4. J. E. Doninger and W. F. Stevens, *A.I.Ch.E. J.*, **14**, 591 (1968).
5. S. D. Conte and R. T. Dames, *Math. Aids Comp.*, **12**, 198 (1958).
6. C. V. McSwain, Ph.D. dissertation, Texas A&M University, College Station, Texas, 1968.
7. B. C. Kuo, *Automatic Control Systems*, Prentice-Hall, Englewood Cliffs, N.J., 1962.
8. L. N. G. Filon, *Proc. Roy. Soc. (Edinburgh)*, **49**, 38 (1928).
9. M. I. Brittan and E. T. Woodburn, *A.I.Ch.E. J.*, **12**, 541 (1966).
10. M. H. Roemer and L. D. Durbin, *Ind. Eng. Chem. Fundamentals*, **6**, 120 (1967).
11. J. H. Perry (ed.), *Chemical Engineers Handbook*, 3rd ed., McGraw-Hill, New York, 1950, p. 674.

Received by editor September 10, 1968
Submitted for publication December 20, 1968